Efficiency Conceptualization Model: A Theoretical Method for Predicting the Turnover of Catalysts

Himangshu Pratim Bhattacharyya, Manabendra Sarma*

In recent times, the theoretical prediction of catalytic efficiency is of utmost urgency. With the advent of density functional theory (DFT), reliable computations are possible that delineate a quantitative aspect of the study. To this state-of-the-art approach, valuable incorporation would be a tool that can acknowledge the efficiency of a catalyst. In the current work, we developed a method, the efficiency conceptualization model (ECM), that utilizes the quantum mechanical tool to achieve efficiency in terms of turnover frequency (TOF). For the convenience of comparison, all calculations and relations were implemented under the experimental conditions of temperature, pressure, and pH. In the current work, ECM will be executed for the water-oxidation reaction with twenty-six experimentally synthesized transition metal catalysts. The results suggest that the iron (Fe)-based catalysts (MWOC-16, MWOC-17, and MWOC-18) are highly active catalysts and therefore can withstand for more time in the catalytic cycle. Our results conclude that the iridium (Ir) based catalysts MWOC-23 and MWOC-24 report the highest computed turnover number, $\tau^0_{computed\ TON}$ of 5113 and 5612 against the highest experimental TON, $\tau_{experimental\ TON}$ of 2000 and 1200 respectively, whereas MWOC-19 has the lowest computed TON ($\tau^0_{computed\ TON} = 264$, $\tau_{experimental\ TON} = 16$) among the chosen catalysts and thereby is successful in corroborating the previous experimental results.

Introduction

The turnover frequency (TOF) is a significant parameter to evaluate the efficiency of designed catalysts. In an experimental reaction, the TOF of designed catalysts can not be predetermined. Considering the inadequacy, the development of a novel strategy to predict the TOF is highly desirable. To compute the mechanism and catalytic activity, computations with the energetic span model [1,2], degree of rate control [3,4], molecular volcano plots [5], and microkinetic modelling [6], NaviCatGA [7] have been very useful.

Although, substantial attempts have been made to design new methods that have high turnover frequencies, however, the strategies to forecast the same involve considerable inadequacies. The theoretical methods or computational results are often anticipated to replicate experimental findings. However, it is worth mentioning that the connection between the theory and experiment is not always necessary and obvious as the "language" of both the disciplines are different as aptly mentioned by Kozuch *et al.* [1] Considering all the facts, based on the kinetic and thermodynamic perspectives involved in the rate-limiting process we developed a mathematical model, namely efficiency conceptualization model (ECM) to compute turnover frequency, $\Gamma^0_{computed\ TOF}$ and is considered as the central theme of this work. For a comparative study, we define turnover frequency ($\Gamma^0_{computed\ TOF}$) under the experimental conditions of temperature, pressure, and pH. The ECM will be extended to compute the turnover number, $\tau^0_{computed\ TON}$ of the twenty-six transition metal-based catalysts involved in the water-oxidation reaction. We hope the research paradigm presented in this work may be applicable in exploring TONs of the general catalytic reactions. The roadmap to ECM is shown in Scheme 1.

Developing the Method: Basis of Constructing the Equations

Kinetic Perspectives: Rate Constants and Tunneling Phenomena

For any rate-determining step (RDS) of a chemical reaction with molecularity n,

$$\mathbf{nR} \xrightarrow{k_1} \mathbf{P}$$

The rate of the reaction depends on the concentration of the reacting species involved in the RDS and can be expressed as

$$rate \propto [R]^n \tag{1}$$

$$rate = k_1[R]^n \tag{2}$$

The rate constant k_1 is derived from the transition state theory (TST) [8–10] that would be observed without considering the quantum effects and is given as

$$k_1 = \frac{k_B T}{hc^o}\ exp\left(-\frac{\Delta G_a}{RT}\right) \tag{3}$$

Where c^0 = standard concentration (taken as 1 M in the present case), ΔG_a is the standard Gibbs energy of activation, k_B is the Boltzmann's constant, R is the universal gas constant, h is the Planck's constant, and T is the temperature.

The reaction coordinate for the targeted reaction may involve substantial motion of light atoms in its transition-state (TS) geometry. Therefore, one may consider the overall reaction rate constant, $k_{overall}(T)$, to include a significant contribution from light-atom tunneling, even at typical

[] H. P. Bhattacharyya, Dr. M. Sarma*
Department of Chemistry, Indian Institute of Technology Guwahati, Assam-781039, India
E-mail: msarma@iitg.ac.in

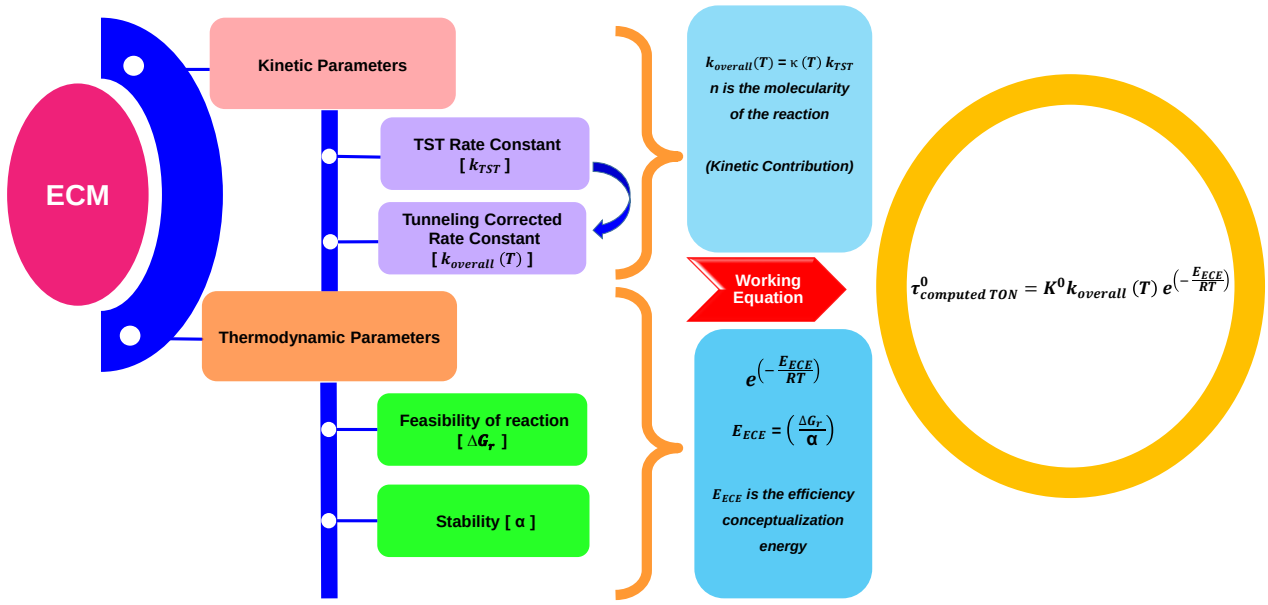

Scheme 1. Roadmap to efficiency conceptualization model (ECM).

room temperature (298.15 K). Considering the fact, the rate of the reaction is expressed as [11,12]

$$rate = \kappa(T) k_1 [R]^n \tag{4}$$

$$rate = k_{overall}(T)[R]^n \tag{5}$$

Where,

$$k_{overall}(T) = \kappa(T)\ k_1 \tag{6}$$

Where $\kappa(T)$ is the quantum mechanical transmission coefficient.

To compute the transmission coefficient, $\kappa(T)$, the efficiency conceptualization model (ECM) considers the one-dimensional Wigner tunneling method [13] and the Eckart tunneling method. [14,15] The value can be computed in light of the Wigner tunneling method [13] using Eq. (7)

$$\kappa(T) = 1 + \frac{1}{24}\left(\frac{h\omega^*}{k_B T}\right)^2 \tag{7}$$

However, the Wigner tunneling method does not account for the barrier height of the reaction profile, and therefore, lacks the accuracy to evaluate $\kappa(T)$. [11] Hence, to address the barrier height, the Eckart tunneling method is one of the viable alternatives to calculate the transmission coefficient, $\kappa(T)$. Thus, in the RDS, in the light of the Eckart tunneling method, the $\kappa(T)$ can be expressed as the ratio of thermally averaged quantum tunneling probability to the quasi-classical transmission probability given by

$$\kappa(T) = \frac{\int_{E_0}^{\infty} P^T(E) e^{-E/k_B T}}{\int_{E_0}^{\infty} P^C(E) e^{-E/k_B T}} \tag{8}$$

In Eq. (8), E_0 is the ground vibrational state energy of the stationary points (reactant or product) at typical room temperature, and E is the system's total energy. P^C(E) is the probability obtained from the TST rates, and P^T(E) is the quantum tunneling probability. The P^T(E) can be defined as [11]

$$P^T(E) = 1 - \left[\frac{cosh[2\pi(\alpha - \beta) + cosh[2\pi\delta]}{cosh[2\pi(\alpha + \beta) + cosh[2\pi\delta]}\right] \tag{9}$$

The equations related to Eq. (9) were provided in Supporting Information S1.

A reaction with a higher overall rate constant, $k_{overall}$ suggests a faster pre-equilibrium in the catalytic cycle. [1] In other words, the higher overall rate constant, $k_{overall}(T)$ indicates more catalytic cycles completed by the catalyst. This, in turn, raises the value of computed turnover frequency, $\Gamma^0_{computed\ TOF}$. Thus, the $\Gamma^0_{computed\ TOF}$ of a reaction is directly proportional to the $k_{overall}(T)$ of the reaction as

$$\Gamma^0_{computed\ TOF} \propto k_{overall}(T) \tag{10}$$

Thermodynamic Perspectives: Efficiency Conceptualization Energy

The $\Gamma^0_{computed\ TOF}$ of a catalyst does not depend only on the rate of the reaction but also on the thermodynamic properties of the catalyst. ECM assumes that thermodynamically, two factors, *viz.*, feasibility of the reaction (ΔG_r) and stability (α) of the catalyst complex, to be addressed that affect the $\Gamma^0_{computed\ TOF}$ of the reaction.

The extent of the feasibility of a reaction depends upon the free energy of the reaction, ΔG_r. The feasibility of the reaction is enhanced as the value of ΔG_r becomes more negative. The ΔG_r can be evaluated as

$$\Delta G_r = G_{product} - (G_{reactant} + G_{substrate}) \tag{11}$$

In Eq. (11), ΔG_r is the change in the free energy of the reaction, and $G_{reactant}$, $G_{substrate}$, and $G_{product}$ are the free energies of the reactant, substrate, and product, respectively.

The energy gap between the two frontier orbitals is computationally considered the key feature in explaining the stability of catalysts . Pearson [16] suggested the energy separation between the two frontier orbitals is the measure of the stability of the catalyst. Thus, with an increase in the energy gap, the stability of the catalyst also increase. Mathematically,

$$\alpha = E_{HOMO} - E_{LUMO} \tag{12}$$

Where LUMO is the lowest unoccupied molecular orbital, and HOMO is the highest occupied molecular orbital.

The efficiency conceptualization model (ECM) combines the two thermodynamic parameters *viz.*, feasibility of the reaction (ΔG_r) and stability (α) of a catalyst to define a new term, efficiency conceptualization energy (E_{ECE}), that describes the threshold thermodynamic energy of the catalyzed reaction. The ECM further proposed that the value of E_{ECE} will enhance with an increase in the ΔG_r and decrease with the stability (α) of the catalyst. Thus,

$$E_{ECE} = \left(\frac{\Delta G_r}{\alpha}\right) \times E^o \tag{13}$$

Where E^0 is the proportionality constant, and in the present case, under standard conditions of temperature and pressure, it is assumed to be 1 unit.

Computing Turnover Frequencies

The feasibility (ΔG_r) of a reaction is inversely related to the $\Gamma^0_{computed\ TOF}$ of the catalyst.[17] With increasing stability (*i.e.*the HOMO-LUMO energy gap) it is difficult to excite an electron. Thus, the ECM assumes that the $\Gamma^0_{computed\ TOF}$ of the catalyst varies directly with the stability of a catalyst. Thus,

$$\Gamma^0_{computed\ TOF} \propto f\left(\frac{\alpha}{\Delta G_r}\right) \tag{14}$$

Thus, comparing Eq. (13) and Eq. (14), we have

$$\Gamma^0_{computed\ TOF} \propto f(\frac{1}{E_{ECE}}) \tag{15}$$

Further, the $\Gamma^0_{computed\ TOF}$ of a catalyst is proportional to the fraction of molecules $\left(\frac{N}{N_0}\right)$, where N is the number of molecules that possess threshold thermodynamic energy, E_{ECE} and N_0 is total number of molecules. Thus, with an increase in the fraction of molecules, the $\Gamma^0_{computed\ TOF}$ of the catalyst varies as

$$\Gamma^0_{computed\ TOF} \propto \left(\frac{N}{N_0}\right) \tag{16}$$

Among the available N_0 molecules, all molecules may not lead to product formation. Only the $\left(\frac{N}{N_0}\right)$ fraction of molecules that possess the threshold thermodynamic energy E_{ECE} will contribute to $\Gamma^0_{computed\ TOF}$. Thus, analogous to the Boltzmann distribution[18], we have

$$\left(\frac{N}{N_0}\right) \propto exp\left(-\frac{E_{ECE}}{RT}\right) \tag{17}$$

Thus, from Eq. (16) and Eq. (17), we can have

$$\Gamma^0_{computed\ TOF} \propto exp\left(-\frac{E_{ECE}}{RT}\right) \tag{18}$$

Therefore, by combining Eq. (10) and Eq. (18), we have

$$\Gamma^0_{computed\ TOF} \propto k_{overall} \times exp\left(-\frac{E_{ECE}}{RT}\right) \tag{19}$$

or,

$$\Gamma^0_{computed\ TOF} = K^0 k_{overall} \times exp\left(-\frac{E_{ECE}}{RT}\right) \tag{20}$$

In Eq. (20), the value of K^0 is assumed to be 1 unit under standard temperature and pressure conditions. However, the value of K^0 may vary based on the reaction conditions and type of reaction.

Extended ECM Theory: Predicting Half-lives and Turnover Numbers.

The efficiency conceptualization model (ECM) was further extended in order to compute the turnover number (TON), $\tau^0_{computed\ TON}$ of the catalyst. The $\tau^0_{computed\ TOF}$ of a catalyst is related to the half-life ($t_{\frac{1}{2}}$) and of the complex as[19]

$$\tau^0_{computed\ TON} = \frac{\Gamma^0_{computed\ TOF} \times t_{\frac{1}{2}}}{ln2} \tag{21}$$

The half-life of the complex ($t_{\frac{1}{2}}$) can be calculated by (Supporting Information S1)

$$t_{\frac{1}{2}} = \frac{2ln2 + [c]_0 e^{-\frac{\Delta G_r}{RT}}}{2k_1[R]_0} \tag{22}$$

In Eq. (22), for the considered rate-determining step, k_1 is the TST rate constant, $[R]_0$ is the initial concentration (1 M) of the reactant, ΔG_r is the change in the free energy of reaction, R is the universal gas constant, T is the typical room temperature. During a catalyzed reaction, the reactant concentration is much higher than that of the catalyst concentration.[19–21] In our computations, in comparison to the initial reactant concentration of 1 M, the initial catalyst concentration, $[c]_0$ is assumed to be 1 mM. Nevertheless, the catalyst concentration may be varied and accordingly, values may be computed.

Thus, using the values of $\Gamma^0_{computed\ TOF}$ [Eq. (20)] and half-life of the catalysts ($t_{\frac{1}{2}}$) [Eq. (22)] in Eq. (21), the turnover frequency (TOF), $\Gamma^0_{computed\ TOF}$ of catalysts under experimental conditions of temperature, pressure, and pH may be obtained.

Execution of the Model: Application to Transition-Metal-based Molecular Water-Oxidation Catalysts (MWOCs)

To address the energy proposition in the global scenario, the artificial splitting of water is considered one of the suitable alternatives for clean and sustainable energy.[22,23] However, artificial water splitting is an energetically uphill process (ΔG = 237 kJ/mol)[24] and requires the designing of a robust and efficient catalyst that can initiate the loss of $4H^+/4e^-$ with simultaneous formation of O-O bond.[25] In nature, the observed excellent efficiency of the water oxidation process was triggered at the oxygen-evolving center (OEC) catalyzed by the tetra-manganese cluster (Mn_4CaO_5) of the photosystem II (PSII), as shown in Figure 1(a).[26–29]

Throughout the last few decades, substantial efforts related to the synthesis, mechanism, electronic structure, oxidation states, and spectroscopic studies of the natural photosynthetic system have been endowed.[30–37] Synchronously, to accomplish the goal of impersonating the natural photosynthetic system, *in vitro* synthesis of robust catalysts with high turnover numbers (TONs) and lower over-potential, there is a high interest in the transition elements.[38–48] Of

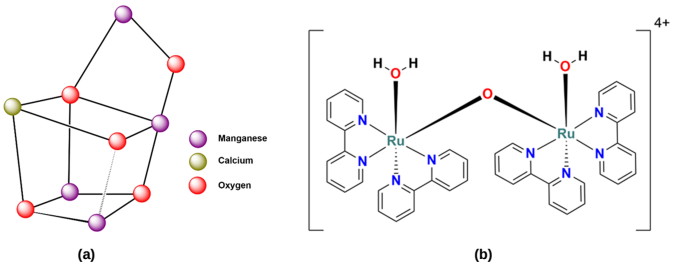

Figure 1. (a) Natural multi-metallic Mn_4CaO_5 core of oxygen evolving center (OEC); (b) structure of the blue dimer, cis,cis-$[Ru^{II}(bpy)_2(H_2O)]_2(\mu\text{-}O)]^{4+}$.

the various mononuclear transition metal catalysts, ruthenium (Ru) active centers were extensively studied [49–53] because of their lucid structure and diagonal relationship to the manganese (Mn) center. [22,27] The first biomimetic catalyst cis, cis-$[Ru^{II}(bpy)_2(H_2O)]_2(\mu\text{-}O)]^{4+}$ [Figure 1(b)] (blue dimer) was reported by Meyer and co-workers. [54–56] For water oxidation, the second (4d) and third-row (5d) transition elements, such as ruthenium (Ru) and iridium (Ir), have been known for their high activity and robustness. [20,23,57,58] However, the earth-abundant and cost-effective first-row (3d) transition elements can also operate water oxidation under mild conditions. Although extensive research has been carried out on the catalysts based on manganese (Mn) [38–40,59], iron (Fe) [21,60–62], cobalt (Co) [63,64], nickel (Ni) [47,65], and copper (Cu) [8,46,66,67], however, these catalysts need a high formal oxidation state. These led to the first row of elements being a more apt catalytic system than Ru-based catalysts. However, rational design and synthesis of the water oxidation catalysts with 3d-transition elements as an active center requires further exploration.

In the current work, to execute the strategy, as an initial illustration, for probing the $\Gamma^0_{computed\ TOF}$, we considered twenty-six transition-metal-based molecular water-oxidation catalysts (MWOCs) as shown in Figure 2.

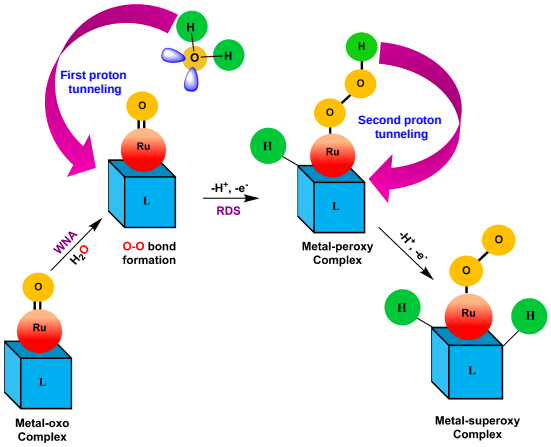

Scheme 2. Rate determining step (RDS) of the O-O bond formation process via water nucleophilic attack (WNA) mechanism. The protons from water tunnel to different parts of the ligand (L).

Computationally, Baik *et al.* have discussed the stability and reactivity of the $[Mn(V){=}O]^+$ species, explored oxyl radical's magnitude, and analyzed its relation to spin state and oxidation states. [39] Li *et al.* have proposed that the $[Mn(Py_2NR_2)(H_2O)]^{2+}$ with R = ^{t}Bu has an equal proba-

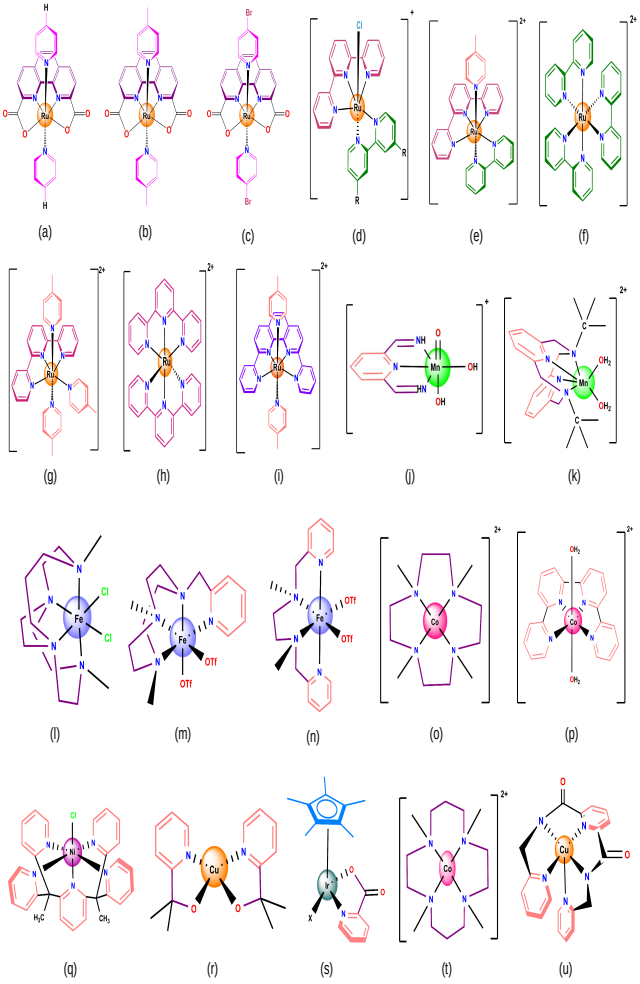

Figure 2. Structures of the representative twenty-six catalysts with (a) MWOC-1: $[Ru(pda)(py)_2]$; (b) MWOC-2: $[Ru(pda)(pic)_2]$; (c) MWOC-3: $[Ru(pda)(Br\text{-}py)_2]$; (d) Derivatives of $[Ru(bpy)(tpy)Cl]^+$ with MWOC-4: R= -H ; MWOC-5: R = Methyl (-Me) ; MWOC-6: R= Methoxy (-OMe) ; MWOC-7: R= Nitro ($-NO_2$) ; and MWOC-8: R= Ethoxycarbonyl (-COOEt) ; (e) MWOC-9: $[Ru(tpy)(bpy)(pic)]^{2+}$; (f) MWOC-10: $[Ru(bpy)_3]^{2+}$; (g) MWOC-11: $[Ru(tpy)(pic)_3]^{2+}$; (h) MWOC-12: $[Ru(tpy)_2]^{2+}$; (i) MWOC-13: $[Ru(dpp)(pic)_2]^{2+}$; (j) MWOC-14: $[Mn(Py)(O)(OH)_2]^+$; (k) MWOC-15: $[Mn(Py)_2NR_2(H_2O)_2]^{2+}$] with R = ^{t}Bu ; (l) MWOC-16: cis-$[Fe(cbc)Cl_2]^+$; (m) MWOC-17: $[Fe(OTf)_2(Me_2Pytacn)]$; (n) MWOC-18: $[Fe(OTf)_2(mep)]$; (o) MWOC-19: $[Co(12\text{-}TMC)]^{2+}$; (p) MWOC-20: trans-$[Co(qpy)_2(OH_2)_2]^{2+}$; (q) MWOC-21: Ni-PY5 ; (r) MWOC-22: $[Cu(pyalk)_2]$; (s) $[Cp^*Ir(\kappa^2\text{-}N,O)X]$ with MWOC-23: X = Cl ; and MWOC-24: X = NO_3 ; (t) MWOC-25: $[Co(13\text{-}TMC)]^{2+}$; (u) MWOC-26: $[Cu(Py_3P)]$.(Where, pda = 1,10-phenanthroline-2,9-dicarboxylate; pic = 4-picoline; py = pyridine; Br-py = 4-Bromopyridine; bpy = 2,2′-bipyridine; tpy = 2,2′:6′,2′′-terpyridine ; dpp = 2,9-dipyrid-2′-yl-1,10-phenanthroline; Py = pyridinophane; cbc = 4,11-dimethyl-1,4,8,11-tetraazabicyclo[6.6.2]hexadecane ; OTf = $CF_3SO_3^-$; $Me_2Pytacn$ = 1-(2′-pyridylmethyl)-4,7-dimethyl-1,4,7-triazacyclononane; mep = N,N′-dimethyl- N,N′-bis-(2-pyridylmethyl)-ethane-1,2-diamine; 12-TMC = 1,4,7,10-tetramethyl-1,4,7,10-tetraazacyclododecane; qpy = 2,2′:6′,2′′:6′′,2′′′-quaterpyridine; PY5 =2,6-bis(1,1-bis(2-pyridyl)ethyl)pyridine; pyalk = 2-pyridyl-2-propanoate; κ^2-N,O = 2-pyridinecarboxylate, 13-TMC = 1,4,7,10-tetramethyl-1,4,7,10-tetraazacyclotridecane, Py_3P = N,N -bis(2-(2-pyridyl)ethyl)pyridine-2,6-dicarboxamidate.)

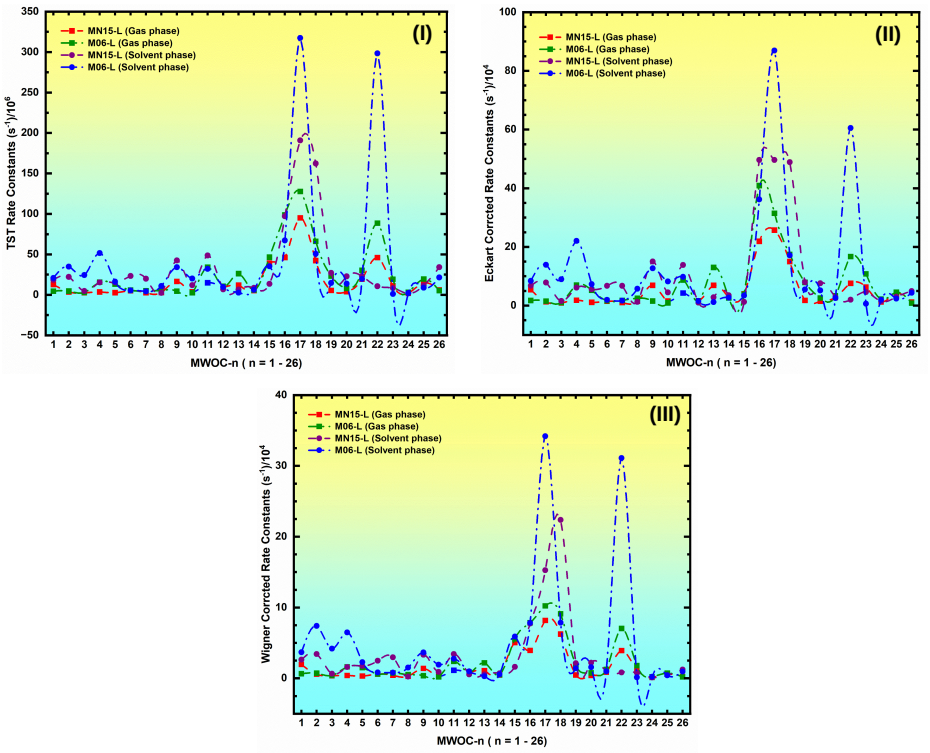

Figure 3. (I) TST rate constants (s^{-1}), (II) Eckart tunneling corrected rate constants (s^{-1}), and (III) Wigner tunneling corrected rate constants (s^{-1}) for twenty-six catalysts in solvent phase using the solvation model density (SMD).[68] MN15-L[69] and M06-L[70] functionals were employed with LANL2DZ effective core potential (ECP) for all the metal (M) atoms (M = Mn, Fe, Co, Ni, Cu, Ru, and Ir) and Br atom, and 6-31G(d) basis set for all other elements.

bility for the water nucleophilic mechanism (WNA) and OH-OH coupling.[71] The iron complexes with neutral tetradentate ligands in cis-labile positions for water oxidation were computationally reported by Lloret-Fillol *et al.*[21] They reported the iron complexes to follow two different mechanisms and the water-nucleophilic attack (WNA) pathway is found to be favourable with a lower energy barrier.[21] Further, they computationally justified that for the modelling of the O-O bond formation, four water molecules are necessary via the external water nucleophilic attack pathway in which the Fe(V)=O intermediate is energetically more accessible than the Fe(IV)=O intermediate.[21] Rudshteyn *et al.* investigated the plausible water oxidation mechanism of the copper (Cu) catalyst, which is catalytically active in isomeric form.[8] The proposed mechanism suggests that shuttling over multiple oxidation states is necessary for efficient water oxidation. Herein, we have exclusively considered the catalysts that follow water oxidation via the water-nucleophilic attack (WNA) pathway as illustrated in Scheme 2.

Results and Discussion

Transition State Theory and Tunneling Corrected Rate Constants

The transition states for twenty-six catalysts have been evaluated in both MN15-L[69] and M06-L[70] levels of theories. The computed transition states were characterized by one imaginary frequency and reported in Supporting Information S11. The barrier heights computed for the O-O bond formation (Scheme 2) from the difference in free energies of the transition state and the reactant. Thus, with the obtained free energies (ΔG_a), k_1 for the O-O bond formation process evaluated using the transition-state theory[8–10] given by Eq. (2). The obtained rate constants are displayed in Figure 3(I) and reported in Table S6A-S6B of Supporting Information S6. Our calculation shows that kinetically MWOC-17 shows a higher rate of reaction in both the MN15-L and M06-L level of theories.

The obtained TST rate constants for the rate-limiting O-O bond formation process (Scheme 2) was further corrected to evaluate $\kappa(T)$ using the one-dimensional Eckart tunneling method[14,15] and Wigner tunneling method[13]. For both Eckart and Wigner methods, the rate constant of catalysts enhances ∼100 times (from 10^{-6} to 10^{-4}) than that of the TST rate constants. The results for the TST rate constants, Eckart and Wigner tunneled rate constants are shown in Figure 3.

Feasibility of Reaction and Stability of Catalysts

As mentioned in Eq.(14), the efficiency conceptualization energy (E_{ECE}) depends on the feasibility (ΔG_r) and stability (α) of the catalyst. We found that the feasibility of the water oxidation reaction depends upon the energetics of the lowest unoccupied molecular orbital (LUMO), E_{LUMO}, of the formed metal-oxo $[M^V{=}O]^{(n+1)+}$ species.

According to Pearson[16], the energy of the LUMO can be correlated to the electron affinity (EA) as E_{EA} = -E_{LUMO}, which determines the strength of the O-O bond formation (OBF). In our study, for both MN15-L and M06-L level of theories, the metal-oxo form of MWOC-19 has more negative Gibbs free energy than the remaining catalysts. Fur-

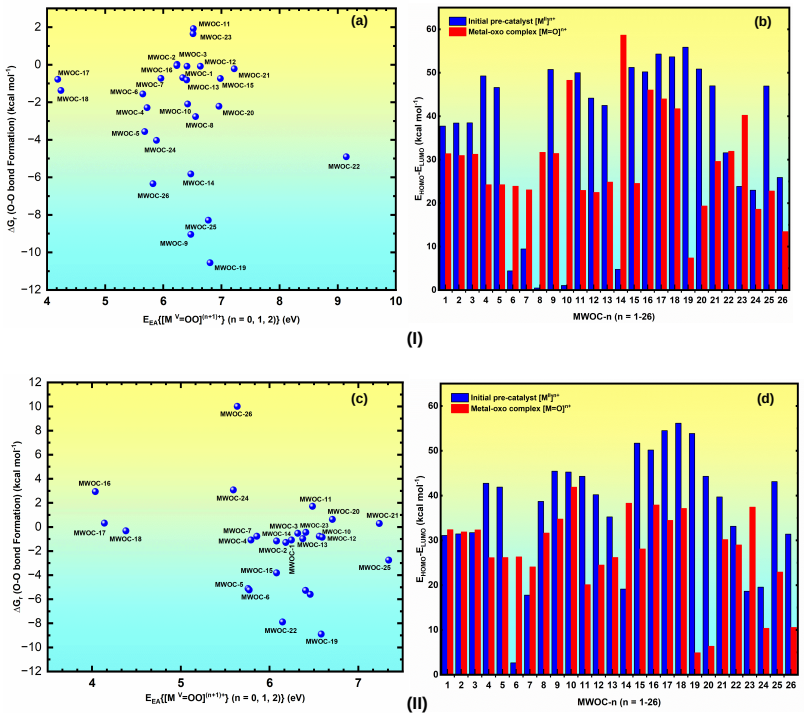

Figure 4. Variations in the (I) in the MN15-L functional (a) feasibility of the reaction, ΔG_r (O-O bond formation) in solvent phase (in kcal mol^{-1}); (b) comparison of stability $[M^{II}]^{n+}$ and corresponding metal oxo, $[M^{V}{=}O]^{n+1}$ (n =0, 1, 2) form and (II) in the M06-L functional (c) feasibility of the reaction, ΔG_r (O-O bond formation) in solvent phase (in kcal mol^{-1}); (d) comparison of stability $[M^{II}]^{n+}$ and corresponding metal oxo, $[M^{V}{=}O]^{(n+1)+}$ (n =0, 1, 2) form of representative twenty-six catalysts. For each functional LANL2DZ effective core potential (ECP) for all the metal (M) atoms (M = Mn, Fe, Co, Ni, Cu, Ru, and Ir) and Br atom, and 6-31G(d) [72–74] basis set for all other atoms. The blue and red bars indicate the HOMO-LUMO energy gap for $[M^{II}]^{n+}$ and $[M^{V}{=}O]^{n+1}$ (n =0, 1, 2) complexes, respectively.

ther, MWOC-19 possesses comparatively high electron affinity, thereby making the reaction feasible [Figure 4 (a) and (c)].

To investigate the stability, the $[M^{V}{=}O]^{(n+1)+}$ complex (M = Mn, Fe, Co, Ni, Cu, Ru, and Ir; and n = 0, 1, 2) with the initial pre-catalyst form $[M^{II}]^{n+}$ were compared. The energy gap in the metal-oxo complex, $[M^{V}{=}O]^{(n+1)+}$ is less relative to its catalyst form, $[M^{II}]^{n+}$ (M = Mn, Fe, Co, Ni, Cu, Ru, and Ir; and n = 0, 1, 2). Thus, the formed metal-oxo complex, $[M^{V}{=}O]^{(n+1)+}$ (M = Mn, Fe, Co, Ni, Cu, Ru, and Ir; and n = 0, 1, 2) loses its stability and simultaneously enhances its activity compared to its catalyst form. However, to compute TONs, out of the two different catalytic forms of the catalyst, we will consider the $[M^{V}{=}O]^{(n+1)+}$ (M = Mn, Fe, Co, Ni, Cu, Ru, and Ir; n = 0, 1, 2) form of the catalyst as it acts as the reactant in the rate-determining step of the O-O bond formation, as shown in Scheme 2. Among catalysts, the $[M^{V}{=}O]^{(n+1)+}$ (n = 0, 1, 2) form of MWOC-14 has a high HOMO-LUMO energy gap (58.66 kcal mol^{-1}) and acts as a stable catalyst and has a lower reactivity. However, for MWOC-19, the HOMO-LUMO energy gap is very small and thus leads to lower stability and higher reactivity. [75]

Computing TONs, TOFs and Its Validation with the Experiment.

To calculate the turnover frequency ($\Gamma^{0}_{computed\ TOF}$) for individual catalysts under experimental conditions of temperature, pressure, and pH, we adopted Eq. (20) and extended ECM to calculate the turnover numbers (TONs), $\tau^{0}_{computed\ TON}$ using Eq. (21) and were reported in Table 1.

Table 1. Computed TOFs ($\Gamma^{0}_{computed\ TOF}$) and TONs ($\tau^{0}_{computed\ TON}$) with ECM in MN15-L levels of theories. The TOFs were reported in s^{-1}.

MWOC	$\Gamma^{0}_{computed\ TOF} \times 10^{5}$ (s^{-1})	$\tau^{0}_{computed\ TON}$
MWOC-16	495.00	5107
MWOC-17	481.00	2520
MWOC-18	463.00	2860
MWOC-11	120.00	2476
MWOC-9	92.30	2171
MWOC-2	78.10	3516
MWOC-1	65.40	3520
MWOC-7	64.10	3237
MWOC- 20	62.60	2737
MWOC-6	60.30	2576
MWOC-4	52.30	3419
MWOC-5	43.40	2837
MWOC-23	43.00	5113
MWOC-10	42.00	3503
MWOC-14	29.70	3471
MWOC-21	28.10	1221
MWOC-13	26.70	4045
MWOC-26	22.30	656
MWOC-25	16.20	1396
MWOC-22	15.60	1486
MWOC-3	15.30	3179
MWOC-15	12.00	883
MWOC-8	10.80	4286
MWOC-12	10.10	1487
MWOC-24	9.87	5612
MWOC-19	7.14	264

Computed TOF

[c] experimentally not reported

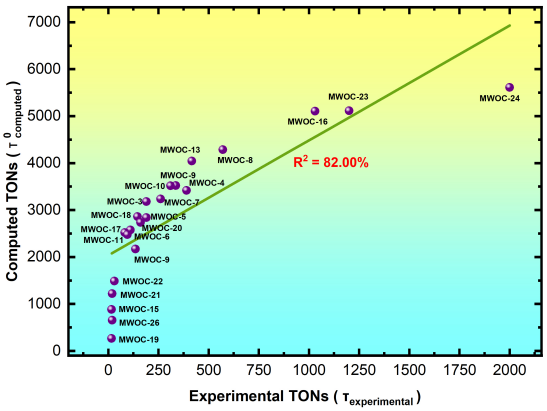

Figure 5. Linear fitting between computed TONs, $\tau^0_{computed\ TON}$ and experimental TONs, $\tau_{experimental\ TON}$ at the MN15-L level of theory.

To understand the extent of degradation, the activity of the catalysts was judged by calculating the catalysts' turnover frequency (TOF). Our computed results concludes that the iron (Fe)-based catalyst MWOC-16, MWOC-17, and MWOC-18 complexes showed the highest $\Gamma^0_{computed\ TOF}$ of 495 $\times$ 10^{-5} s^{-1}, 481 $\times$ 10^{-5} s^{-1} and 463 $\times$ 10^{-5} s^{-1} respectively in MN15-L level of theory under experimental conditions of temperature, pressure, and pH. Thus, the computed results further suggest that the MWOC-16 is a highly active catalyst and can withstand a longer time in the catalytic cycle.

It is important to mention that a higher turnover frequency (TOF) of a catalyst does not always assure a higher turnover number (TON). On extending the strategy, our computations showed that the iridium (Ir) based catalysts with MWOC-23 and MWOC-24 report the highest turnover number, $\tau^0_{computed\ TON}$ of 5113 and 5612 against the highest experimental TON, $\tau_{experimental\ TON}$ of 1200 and 2000 [57] respectively in the MN15-L level of theory.

Further, the results also delineate MWOC-19 to have the lowest value of computed TON, $\tau^0_{computed\ TON}$ = 264 ($\tau_{experimental}$ = 19) [64] in the same level of theory corroborating the previous experimental results. Thus, the method successfully defines the catalytic activity of catalysts and computed TONs.

To observe the validity of computed TONs, we carried out a linear fitting analysis and observed that the extended ECM equation uphold a correlation between the computed TONs and the experimental TONs with R^2= 82% as seen in Figure 5. Since the linear fitting for the developed equation shows $R^2 \geq 80\%$, for MN15-L level of theory, the computed results reported to show good fit [76] and thus the results are worth mentioning.

Conclusion

Based on the kinetic and thermodynamic perspectives, we mathematically modelled a new method efficiency conceptualization model (ECM) to predict the TOF ($\Gamma^0_{computed\ TOF}$) of catalysts for any targeted reaction under experimental conditions of temperature, pressure, and pH. To validate the strategy, we started working on the water-oxidation reaction catalyzed by molecular water oxidation catalyst following the WNA pathway. Our computations with ECM conclude with the following new findings –

- For computing the efficiency of catalysts, ECM relies on the rate-determining step (RDS) of the reaction. In context to water oxidation reaction, we focus only on the O-O bond formation process as it is the rate-determining step of the reaction.
- ECM is predicted to uphold for the any reactions irrespective of the molecularity of the reaction.
- ECM demonstrates the fact that the TOF of a catalyst is affected not only by the rate constants of the reaction but also by the reaction's thermodynamic feasibility (ΔG_r) and stability (α). To account for these effects, we have introduced the term efficiency conceptualization energy (E_{ECE}), which describes the threshold thermodynamic energy of a catalyzed reaction.
- The iron (Fe)-based catalysts MWOC-16, MWOC-17, and MWOC-18 show a very high value of computed turnover frequency, $\Gamma^0_{computed\ TOF}$ of 495 $\times$ 10^{-5} s^{-1}, 481 $\times$ 10^{-5} s^{-1} and 463 $\times$ 10^{-5} s^{-1} respectively in MN15-L level of theory under experimental conditions of temperature, pressure, and pH. Thus, the iron-based catalysts are predicted to withstand more in the catalytic cycle. Along the line, under the similar conditions, MWOC-19 shows the least value of $\Gamma^0_{computed\ TOF}$ and thus predicted to get deactivated early in the catalytic cycle.
- The experimental and computed TONs show a good fit and were linearly correlated with an R-squared (R^2) value of 82% in the MN15-L level of theory and is considered to show a good fit.
- The concept of turnover frequency (TOF) was further extended to delineate the turnover numbers (TON) of catalysts. In the context of water oxidation reaction, among the chosen catalysts, the iridium (Ir) based catalysts with MWOC-23 and MWOC-24 report the highest turnover numbers, $\tau^0_{computed\ TON}$ of 5113 and 5612 against the highest experimental TON, $\tau_{experimental\ TON}$ of 1200 and 2000 respectively. In contrast, MWOC-19 showed the lowest value of computed turnover number, $\tau^0_{computed\ TON}$ of 264 against the lowest experimental turnover number $\tau_{experimental\ TON}$ =16 in the MN15-L level of theory and thereby corroborating the previous experimental results.

We hope that the computational approach to the efficiency conceptualization model (ECM) will be a useful tool for catalysis and physical chemists. The strategy provides a lucid mathematical framework to unravel the turnover frequency (TOF) and turnover number (TON) of catalysts. At the current stage, the efficiency conceptualization model (ECM) is implemented under experimental conditions of temperature, pressure, and pH. However, the conditions of temperature, pressure, and concentration will vary, and accordingly, the expression(s) may be amended as required. The discussions in this context will be extended to provide a more detailed understanding of the turning over of catalysts.

Computational Details

The geometry optimization of the $[M^{II}]^{n+}$, $[M^{V}{=}O]^{(n+1)+}$, $[M^{V}{=}O{:}H_2O]^{(n+1)+}$, and $[M^{IV}\text{-}OO]^{n+}$ (M = Mn, Fe, Co, Ni, Cu, Ru, and Ir; n = 0, 1, 2) were performed at the MN15-L[69] and M06-L[70] level of theories with LANL2DZ effective core potential (ECP) for all the metal (M) atoms and Br atom (M = Mn, Fe, Co, Ni, Cu, Ru, and Ir) and 6-31G(d) basis set for all other elements[72–74] using Gaussian 16[77] package. For solvent phase calculations, we adopted the solvation model density (SMD)[68] with water as the medium of interest under the experimental conditions of temperature, pressure, and pH. As far as the density functional theory (DFT) is concerned, the expectation values of the spin operator, $< S^2 >$, increase with a rise in the HF exchange component.[78] To observe the reliability of the MN15-L[69] functional, the spin expectation values, $< S^2 >$,[79] were compared with the M06-L functional and reported in Supporting Information S5. The rate-constants for the water-oxidation were obtained for the twenty-six representative MWOCs in both the gas phase and solvent phase in terms of transition state theory (TST)[9] and further corrected with the Wigner tunneling[13] and Eckart tunneling[14,15] methods. The zero-point corrected Gibbs free energy and the electronic energies of the optimized systems were evaluated at the same computational level of theory. The energies of the optimized geometries were corrected in both MN15-L[69] and M06-L[70] functional with LANL2TZ effective core potential (ECP)[80,81] for all the metal (M) atoms (M = Mn, Fe, Co, Ni, Cu, Ru, and Ir), LANL2DZ for Br, and def2-TZVP[82] basis set for all other atoms. The absolute and relative energies of all the species have been included in Supporting Information S7.

Yamaguchi Broken Spin-Symmetry (BS) Approach.

In the transition metal-catalyzed water oxidation reaction, various reactive intermediates were generated. A single determinant can not explicitly describe the electronic structure of such species. In such cases, the Kohn-Sham density theory failed to explain such phenomena.[83] Therefore, to adopt such situations, we considered the Yamaguchi broken spin-symmetry (BS) approach[84] to determine the energy of spin-purified low spin complexes using the relation

$$^{LS}E = \frac{^{BS}E^{HS} < S^2 > - ^{HS}E^{BS} < S^2 >}{^{HS} < S^2 > - ^{BS} < S^2 >} \qquad (23)$$

In Eq. (23), HS represents the coupled states with high spin and correlates the spin flipping in the low spin state. The $< S^2 >$ is the spin expectation value of the appropriate determinant of the spin operator.

Acknowledgements

The authors acknowledge Supercomputing facility 'PARAM-Ishan' and National Supercomputing Mission (NSM) for providing computing resources of 'PARAM Kamrupa' at IIT Guwahati, which is implemented by C-DAC and supported by the Ministry of Electronics and Information Technology (MeitY) and Department of Science and Technology (DST), Government of India. HPB also thanks DST for the INSPIRE Fellowship (No. DST/INSPIRE Fellowship/2017/IF170899).

Conflict of Interest

The authors declare no conflict of interest.

Keywords: Ab initio calculations • Efficiency Conceptualization Model (ECM)• Homogeneous Catalysis • Turnover Frequency (TOF) • Water splitting

References

[1] S. Kozuch, S. Shaik, *Acc. Chem. Res.* **2011**, *44*, 101.
[2] S. Kozuch, J. M. Martin, *ACS Catal.* **2011**, *1*, 246.
[3] C. Stegelmann, A. Andreasen, C. T. Campbell, *J. Am. Chem. Soc.* **2009**, *131*, 8077.
[4] Z. Mao, C. T. Campbell, *ACS Catal.* **2020**, *10*, 4181.
[5] M. D. Wodrich, B. Sawatlon, M. Busch, C. Corminboeuf, *Acc. Chem. Res.* **2021**, *54*, 1107.
[6] M. Besora, F. Maseras, *WIREs Comput. Mol. Sci.* **2018**, *8*, e1372.
[7] R. Laplaza, S. Gallarati, C. Corminboeuf, *Chem. Methods* **2022**, *2*, e202100107.
[8] B. Rudshteyn, K. J. Fisher, H. M. Lant, K. R. Yang, B. Q. Mercado, G. W. Brudvig, R. H. Crabtree, V. S. Batista, *ACS Catal.* **2018**, *8*, 7952.
[9] D. A. McQuarrie, J. D. Simon, *Physical Chemistry: A Molecular Approach*, volume 1, University science books Sausalito, CA **1997**.
[10] D. G. Truhlar, B. C. Garrett, S. J. Klippenstein, *J. Phys. Chem.* **1996**, *100*, 12771.
[11] J. L. Bao, D. G. Truhlar, *Chem. Soc. Rev.* **2017**, *46*, 7548.
[12] E. C. Sherer, C. J. Cramer, *Organometallics* **2003**, *22*, 1682.
[13] E. P. Wigner, On the quantum correction for thermodynamic equilibrium, in *Part I: Physical Chemistry. Part II: Solid State Physics*, pages 110–120, Springer **1997**.
[14] C. Eckart, *Phys. Rev.* **1930**, *35*, 1303.
[15] H. S. Johnston, J. Heicklen, *J. Phys. Chem.* **1962**, *66*, 532.
[16] R. G. Pearson, *Proc. Natl. Acad. Sci. USA* **1986**, *83*, 8440.
[17] A. Reid, J. Moreno, S. Hooe, K. Baugh, I. Thomas, D. Dickie, C. Machan, *Chem. Sci.* **2022**, *13*, 9595.
[18] S. Wikipedia, B. Llc, B. Group, *Statistical Mechanics: Maxwell-boltzmann Distribution, Brownian Motion, Fick's Laws of Diffusion, Monte Carlo Method, Boltzmann Constant*, General Books LLC **2010**.
[19] S. Kozuch, J. M. Martin, *ACS Catal.* **2012**, *12*, 2787.
[20] L. Tong, L. Duan, Y. Xu, T. Privalov, L. Sun, *Angew. Chem. Int. Ed.* **2011**, *50*, 445.
[21] J. L. Fillol, Z. Codolà, I. Garcia-Bosch, L. Gómez, J. J. Pla, M. Costas, *Nat. Chem.* **2011**, *3*, 807.
[22] D. G. Hetterscheid, J. N. Reek, *Angew. Chem. Int. Ed.* **2012**, *51*, 9740.
[23] T. J. Meyer, *Acc. Chem. Res.* **1989**, *22*, 163.
[24] T. F. Berto, K. E. Sanwald, J. P. Byers, N. D. Browning, O. Y. Gutiérrez, J. A. Lercher, *J. Phys. Chem. Lett.* **2016**, *7*, 4358.
[25] S. Neudeck, S. Maji, I. López, S. Meyer, F. Meyer, A. Llobet, *J. Am. Chem. Soc.* **2014**, *136*, 24.
[26] M. Yagi, M. Kaneko, *Chem. Rev.* **2001**, *101*, 21.

[27] J. D. Blakemore, R. H. Crabtree, G. W. Brudvig, *Chem. Rev.* **2015**, *115*, 12974.
[28] T. A. Corry, P. J. O'malley, *J. Phys. Chem. Lett.* **2018**, *9*, 6269.
[29] S. Luo, I. Rivalta, V. Batista, D. G. Truhlar, *J. Phys. Chem. Lett.* **2011**, *2*, 2629.
[30] Y. Shao, H. J. de Groot, F. Buda, *J. Phys. Chem. Lett.* **2019**, *10*, 7690.
[31] V. Krewald, M. Retegan, F. Neese, W. Lubitz, D. A. Pantazis, N. Cox, *Inorg. Chem.* **2016**, *55*, 488.
[32] M. Pérez-Navarro, F. Neese, W. Lubitz, D. A. Pantazis, N. Cox, *Curr. Opin. Chem. Bio.* **2016**, *31*, 113.
[33] T. Fan, L. Duan, P. Huang, H. Chen, Q. Daniel, M. S. Ahlquist, L. Sun, *ACS Catal.* **2017**, *7*, 2956.
[34] M. A. Hoque, A. D. Chowdhury, S. Maji, J. Benet-Buchholz, M. Z. Ertem, C. Gimbert-Suriñach, G. K. Lahiri, A. Llobet, *Inorg. Chem.* **2021**, *60*, 5791.
[35] M. Schilling, R. A. Cunha, S. Luber, *ACS Catal.* **2020**, *10*, 7657.
[36] M. Gil-Sepulcre, M. Böhler, M. Schilling, F. Bozoglian, C. Bachmann, D. Scherrer, T. Fox, B. Spingler, C. Gimbert-Suriñach, R. Alberto, et al., *ChemSusChem* **2017**, *10*, 4517.
[37] M. Busch, A. Fabrizio, S. Luber, J. Hutter, C. Corminboeuf, *J. Phys. Chem. C* **2018**, *122*, 12404.
[38] W.-T. Lee, S. B. Muñoz III, D. A. Dickie, J. M. Smith, *Angew. Chem. Int. Ed.* **2014**, *53*, 9856.
[39] D. W. Crandell, S. Xu, J. M. Smith, M.-H. Baik, *Inorg. Chem.* **2017**, *56*, 4435.
[40] Y. Naruta, M.-a. Sasayama, T. Sasaki, *Angew. Chem. Int. Ed.* **1994**, *33*, 1839.
[41] M. Okamura, M. Kondo, R. Kuga, Y. Kurashige, T. Yanai, S. Hayami, V. K. Praneeth, M. Yoshida, K. Yoneda, S. Kawata, et al., *Nature* **2016**, *530*, 465.
[42] J. G. Kleingardner, B. Kandemir, K. L. Bren, *J. Am. Chem. Soc.* **2014**, *136*, 4.
[43] B. Kandemir, L. Kubie, Y. Guo, B. Sheldon, K. L. Bren, *Inorg. Chem.* **2016**, *55*, 1355.
[44] W. Lai, R. Cao, G. Dong, S. Shaik, J. Yao, H. Chen, *J. Phys. Chem. Lett.* **2012**, *3*, 2315.
[45] L.-P. Wang, T. Van Voorhis, *J. Phys. Chem. Lett.* **2011**, *2*, 2200.
[46] M.-T. Zhang, Z. Chen, P. Kang, T. J. Meyer, *J. Am. Chem. Soc.* **2013**, *135*, 2048.
[47] D. Wang, G. Ghirlanda, J. P. Allen, *J. Am. Chem. Soc.* **2014**, *136*, 10198.
[48] M. Li, K. Takada, J. I. Goldsmith, S. Bernhard, *Inorg. Chem.* **2016**, *55*, 518.
[49] C. J. Richmond, S. Escayola, A. Poater, *Eur. J. Inorg. Chem.* **2019**, *2019*, 2101.
[50] L. Wang, L. Duan, Y. Wang, M. S. Ahlquist, L. Sun, *Chem. Commun.* **2014**, *50*, 12947.
[51] L. Duan, L. Wang, F. Li, F. Li, L. Sun, *Acc. Chem. Res.* **2015**, *48*, 2084.
[52] Y. Liu, X. Su, W. Guan, L. Yan, *Phys. Chem. Chem. Phys.* **2020**, *22*, 5249.
[53] J. A. Luque-Urrutia, J. M. Kamdar, D. B. Grotjahn, M. Solà, A. Poater, *Dalton Trans.* **2020**, *49*, 14052.
[54] S. W. Gersten, G. J. Samuels, T. J. Meyer, *J. Am. Chem. Soc.* **1982**, *104*, 4029.
[55] J. A. Gilbert, D. S. Eggleston, W. R. Murphy Jr, D. A. Geselowitz, S. W. Gersten, D. J. Hodgson, T. J. Meyer, *J. Am. Chem. Soc.* **1985**, *107*, 3855.
[56] C. W. Chronister, R. A. Binstead, J. Ni, T. J. Meyer, *Inorg. Chem.* **1997**, *36*, 3814.
[57] A. Bucci, A. Savini, L. Rocchigiani, C. Zuccaccia, S. Rizzato, A. Albinati, A. Llobet, A. Macchioni, *Organometallics* **2012**, *31*, 8071.
[58] A. Savini, G. Bellachioma, S. Bolaño, L. Rocchigiani, C. Zuccaccia, D. Zuccaccia, A. Macchioni, *ChemSusChem* **2012**, *5*, 1415.
[59] D. C. Ashley, M.-H. Baik, *ACS Catal.* **2016**, *6*, 7202.
[60] F. Acuña-Parés, M. Costas, J. M. Luis, J. Lloret-Fillol, *Inorg. Chem.* **2014**, *53*, 5474.
[61] T. Liu, B. Zhang, L. Sun, *Chem. Asian J.* **2019**, *14*, 31.
[62] W. C. Ellis, N. D. McDaniel, S. Bernhard, T. J. Collins, *J. Am. Chem. Soc.* **2010**, *132*, 10990.
[63] C.-F. Leung, S.-M. Ng, C.-C. Ko, W.-L. Man, J. Wu, L. Chen, T.-C. Lau, *Energy Environ. Sci.* **2012**, *5*, 7903.
[64] D. Hong, J. Jung, J. Park, Y. Yamada, T. Suenobu, Y.-M. Lee, W. Nam, S. Fukuzumi, *Energy Environ. Sci.* **2012**, *5*, 7606.
[65] M. Zhang, M.-T. Zhang, C. Hou, Z.-F. Ke, T.-B. Lu, *Angew. Chem. Int. Ed.* **2014**, *126*, 13258.
[66] K. J. Young, M. K. Takase, G. W. Brudvig, *Inorg. Chem.* **2013**, *52*, 7615.
[67] S. M. Barnett, K. I. Goldberg, J. M. Mayer, *Nat. Chem.* **2012**, *4*, 498.
[68] A. V. Marenich, C. J. Cramer, D. G. Truhlar, *J. Phys. Chem. B* **2009**, *113*, 6378.
[69] H. S. Yu, X. He, D. G. Truhlar, *J. Chem. Theor. Comput.* **2016**, *12*, 1280.
[70] Y. Zhao, D. G. Truhlar, *J. Chem. Phys.* **2006**, *125*, 194101 (1.
[71] Y.-Y. Li, K. Ye, P. E. Siegbahn, R.-Z. Liao, *ChemSusChem* **2017**, *10*, 903.
[72] R. Ditchfield, W. J. Hehre, J. A. Pople, *J. Chem. Phys.* **1971**, *54*, 724.
[73] D. R. Harper, H. J. Kulik, *Inorg. Chem.* **2022**, *61*, 2186.
[74] R. Kumar, B. Pandey, A. Singh, G. Rajaraman, *Inorg. Chem.* **2021**, *60*, 12085.
[75] C. Deng, R. He, D. Wen, W. Shen, M. Li, *Phys. Chem. Chem. Phys.* **2018**, *20*, 10240.
[76] E. Ostertagová, *Procedia Eng.* **2012**, *48*, 500.
[77] M. J. Frisch, G. W. Trucks, H. B. Schlegel, G. E. Scuseria, M. A. Robb, J. R. Cheeseman, G. Scalmani, V. Barone, G. A. Petersson, H. Nakatsuji, X. Li, M. Caricato, A. V. Marenich, J. Bloino, B. G. Janesko, R. Gomperts, B. Mennucci, H. P. Hratchian, J. V. Ortiz, A. F. Izmaylov, J. L. Sonnenberg, D. Williams-Young, F. Ding, F. Lipparini, F. Egidi, J. Goings, B. Peng, A. Petrone, T. Henderson, D. Ranasinghe, V. G. Zakrzewski, J. Gao, N. Rega, G. Zheng, W. Liang, M. Hada, M. Ehara, K. Toyota, R. Fukuda, J. Hasegawa, M. Ishida, T. Nakajima, Y. Honda, O. Kitao, H. Nakai, T. Vreven, K. Throssell, J. A. Montgomery, Jr., J. E. Peralta, F. Ogliaro, M. J. Bearpark, J. J. Heyd, E. N. Brothers, K. N. Kudin, V. N. Staroverov, T. A. Keith, R. Kobayashi, J. Normand, K. Raghavachari, A. P. Rendell, J. C. Burant, S. S. Iyengar, J. Tomasi, M. Cossi, J. M. Millam, M. Klene, C. Adamo, R. Cammi, J. W. Ochterski, R. L. Martin, K. Morokuma, O. Farkas, J. B. Foresman, D. J. Fox, Gaussian16 Revision C.01 **2016**, gaussian Inc. Wallingford CT.

[78] E. Edler, M. Stein, *Eur. J. Inorg. Chem.* **2014**, *2014*, 3587.
[79] K. A. Moltved, K. P. Kepp, *Chem. Phys. Chem.* **2019**, *20*, 3210.
[80] P. J. Hay, W. R. Wadt, *J. Chem. Phys.* **1985**, *82*, 270.
[81] L. E. Roy, P. J. Hay, R. L. Martin, *J. Chem. Theor. Comput.* **2008**, *4*, 1029.
[82] F. Weigend, R. Ahlrichs, *Phys. Chem. Chem. Phys.* **2005**, *7*, 3297.
[83] G. Zhang, K. Chen, H. Chen, J. Yao, S. Shaik, *Inorg. Chem.* **2013**, *52*, 5088.
[84] K. Yamaguchi, F. Jensen, A. Dorigo, K. Houk, *Chem. Phys. Lett.* **1988**, *149*, 537.

Entry for the Table of Contents

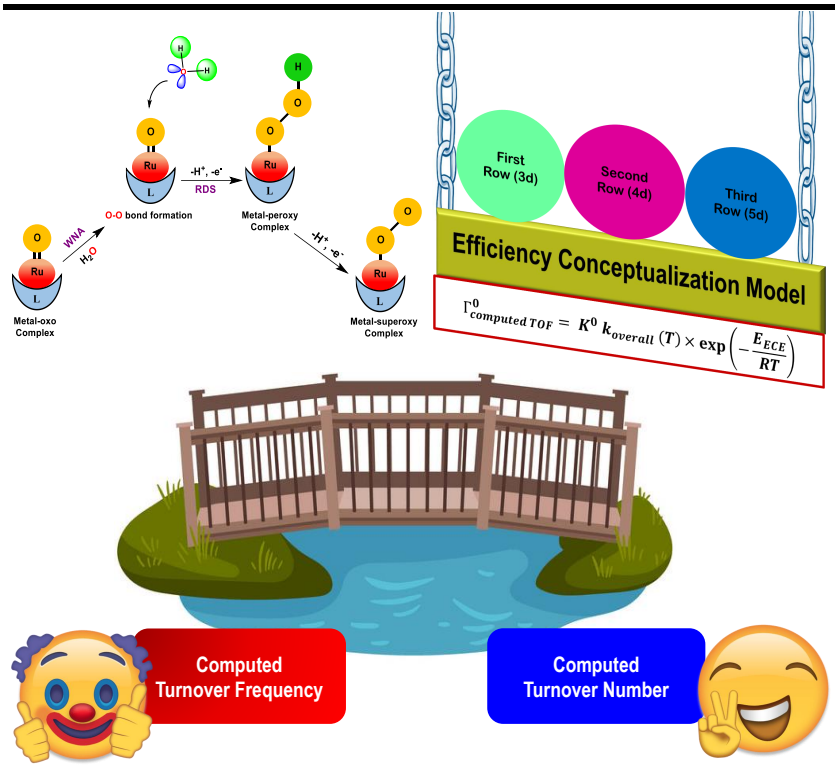

To quantify efficiency, development of a quantum-mechanical tool is very important. Considering the urgency, we developed the efficiency conceptualization model (ECM) that computes turnover frequency (TOF),$\Gamma^0_{computed\ TOF}$ and turnover number (TON),$\tau^0_{computed\ TON}$ of catalysts. To validate the model, we considered the kinetic and thermodynamic aspects of the rate-determining step and applied the same to the first, second, and third-row transition metal-catalyzed water oxidation reaction.